PERGAMON

International Journal of Heat and Mass Transfer 46 (2003) 837–849

International Journal of HEAT and MASS TRANSFER

www.elsevier.com/locate/ijhmt

Turbulent heat transfer and flow characteristics in a horizontal circular tube with strip-type inserts. Part II. Heat transfer

Shou-Shing Hsieh *, Ming-Ho Liu, Huang-Hsiu Tsai

Department of Mechanical and Electro-Mechanical Engineering, National Sun Yat-Sen University, Kaohsiung 80424, Taiwan ROC

Received 3 September 2001; received in revised form 19 August 2002

Abstract

This paper is the second of two papers that presents the results of an extensive study of turbulent heat transfer and pressure drop in a horizontal tubes with strip-type inserts. Experimental data were taken for air for a class of strip inserts (longitudinal strip and crossed-strip). The insert was characterized by the parameters of $1 \leqslant \mathrm{AR} \leqslant 5$ and R^* ($=0.5$ and 1). Friction factor data (from Part I) and temperature measurements were used to understand the underlying physical phenomena responsible for the heat transfer enhancement for $6500 \leqslant Re \leqslant 19\,500$. Nusselt numbers were between four and two times the bare tube values at low Re and high Re, respectively. Performance evaluation index $R1$ (constant pumping power) and $R2$ (constant heat duty) were made and an optimum condition would be thus found.

1. Introduction

The objective of the present two-part study is to experimentally investigate the heat transfer and friction characteristics of air flowing through a horizontal circular tube with strip-type inserts. The first part of the paper addresses flow characteristics, which is responsible for heat transfer enhancement mechanism of the underlying physical phenomena involved in this study.

The range of average temperature of the air used before heated covered in this study varies from 25.5 to 26.5 °C approximately. Two different tube inserts including longitudinal strip (LS) and crossed-strip (CS) with two aspect ratios for LS (CS) were used and shown in Fig. 1. Heat transfer and flow friction data were generated for four different tube inserts under various operating conditions. Relations between the heat transfer capability and the fluid pumping power required are finally presented and discussed.

Part I of this study [1] addressed the fluid mechanics aspects, which explains the underlying physical phenomena responsible for heat transfer enhancement. Flow mechanisms and pressure drop measurements were used to propose friction factor correlation. It is shown in this paper, Part II, that the friction factor correlation of these tubes with inserts can be used in conjunction with heat transfer data to determine the net enhancement effects of this kind of heat transfer device.

2. Experimental setup and procedure

Four tubes with inserts plus one bare tube as shown in Fig. 1 were selected to achieve a wide variation in all the relevant geometric variables. The tubes and geometries dimensions treated here cover almost the same range (four tubes with inserts in Part II) that was included in Part I [1] for the friction factor and pressure drop tests.

Fig. 2 shows a schematic of the test rig. The experiments were performed in an open-loop air flow circuit under the influence of a downstream blower. Air enters the test duct after passing a straightener and flows

* Corresponding author. Tel.: +886-7-525-2000x4215; fax: +886-7-525-4215.

E-mail address: sshsieh@mail.nsysu.edu.tw (S.-S. Hsieh).

0017-9310/03/$ - see front matter © 2002 Elsevier Science Ltd. All rights reserved.
PII: S0017-9310(02)00354-X

Nomenclature

A	cross-sectional area of bare tube (m^2)
AR	aspect ratio, L/H
A_s	heat transfer area (m^2)
C_p	specific heat at constant pressure (J/kg K)
D	tube hydraulic diameter unless otherwise stated (m)
f	friction factor based on the hydraulic diameter, $(\Delta p/(\frac{1}{2}\rho_{air}V^2))(D/\ell)$
g	gravity
Gr^*	modified Grashof number, $g\beta D^4 q''/v^2 k_f$
H	height of insert (m)
h	heat transfer coefficient (W/(m^2 K))
k_f	thermal conductivity of air at film temperature (W/m K)
L	width of insert (m)
ℓ	length of the test tube (m)
Nu	Nusselt number based on the hydraulic diameter, hD/kf
Pr	Prandtl number, v/α
Q_c	conduction heat loss from test section to laboratory environment (W)
Q_{net}	net convection heat flow rate (W)
Q_r	radiation heat loss from test section to laboratory environment (W)
Q_s	the total heat input to the test section (W)
q''	heat flux, Q/A (W/m^2)
R	radius of inner tube (m)
R^*	radius ratio of circumscribed circle of insert to test tube, $0.5(L^2+H^2)^{1/2}/R$
Re	Reynolds number based on the hydraulic diameter, VD/v
T	temperature (K)
T^+	dimensionless temperature, $(T_w - T)/(q''/\rho C_p u^*)$
T^*	dimensionless temperature, $(T - T_{bi})/(Q_{net}/\ell k_f)$
u	velocity in x direction (m/s)
u^*	friction velocity (m/s)
V	nominal (bulk) average velocity (m/s)
x, y	rectangular coordinates
x^*	dimensionless distance in the main flow direction, $(x/D)/(RePr)$
y^+	dimensionless distance from wall in a turbulent shear layer, yu^*/v

Greek symbols

α	thermal diffusivity
β	thermal expansion coefficient; also contraction ratio
η	insert affected coefficient (heat)
ρ	density of working fluid
v	kinematic viscosity

Subscripts

air	air
b	bulk
f	fluid/fully developed
i	inlet
m	total
m, x	local and total
n, x	natural and local
w	wall
x	local position in the main flow direction
o	data from Dittus Boelter's and outside
0	average

Superscripts

+	dimensionless
−	average

through a calibrated flowmeter. Air at room temperature is introduced into the straight horizontal test tube. The test circular tube has inner diameter of 50 and 3000 mm in length. The test tube includes a heating part that has a double-tube structure and is between the tube exit and 3000 mm upstream from the exit. The air temperatures at the inlet and exit of the test section were measured by calibrated thermocouples. Five thermocouples shown in Fig. 3 were used to determine the average air temperature at the inlet and outlet of the test section.

The inner tube of the heating part which is the test tube with inside diameter 50 mm is made of 4 mm-thick aluminum plate. Heating element was filled into the gap between the inner and outer tube with an isoflux condition as desired. The wire (1.8 mm gauge) chosen as a heating element was made of a nickel–chrome alloy. The heating element is 18 mm in diameter. A detail of the manifolds that illustrates the heating element is also shown in Fig. 2. The test inserts were positioned as the same as those in Part I of this paper. The test tube had a fitting added to each end for attachment. The locations of the thermocouples used to measure the test section wall temperature distributions as well as flowing air temperature inside the tube at particular positions are shown in Fig. 3. Temperatures measured at these locations provided experimental confirmation of the establishment of fully developed flow. Fine gauge (1 mm) specially calibrated Cu-Cn thermocouples were employed with the intent of minimizing the disturbance of the temperature field in the vicinity of the thermocouple junctions. The thermocouples were installed in holes

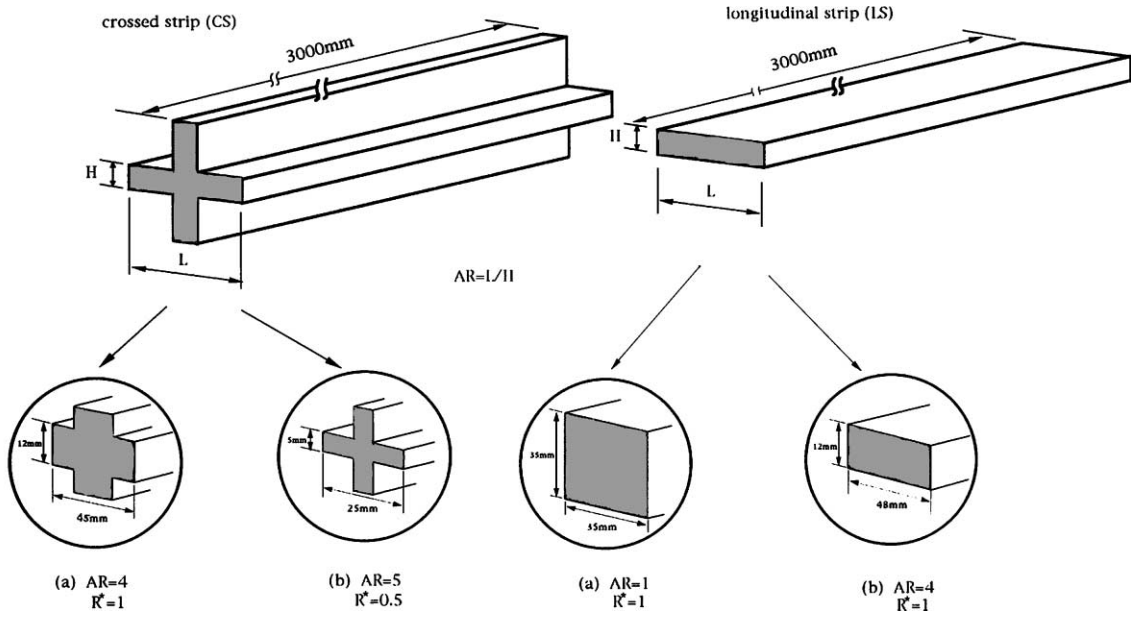

Fig. 1. Physical geometry (LS and CS) and dimensions of the inserts considered.

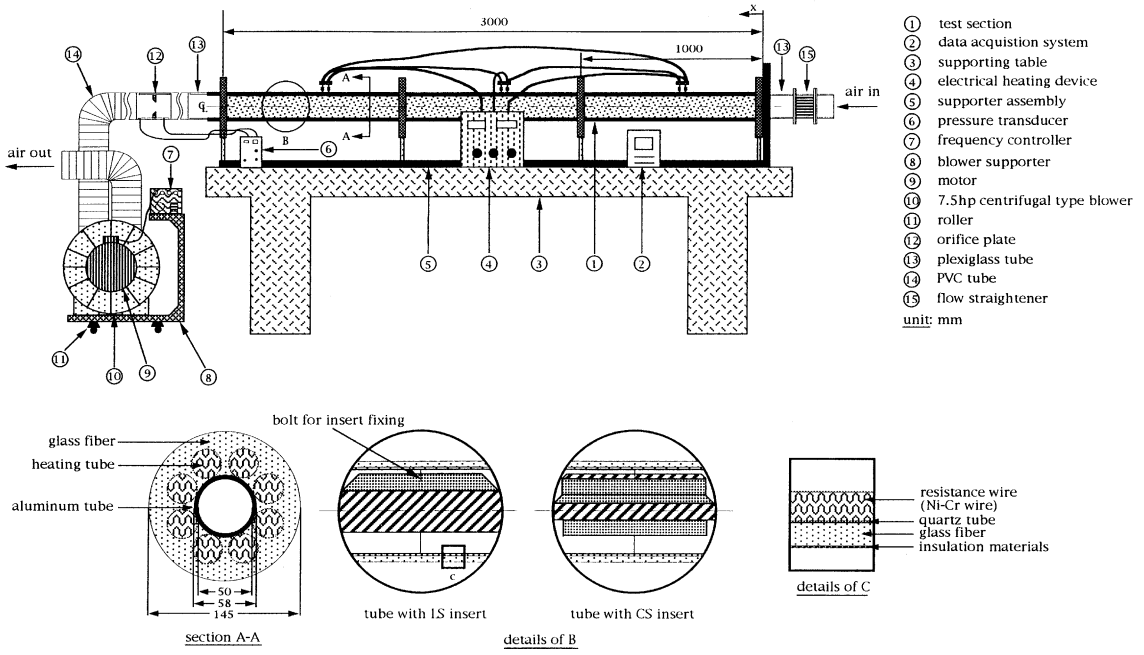

Fig. 2. Schematic of experimental test rig and heating element.

drilled into the back side of the tube walls to within 2 mm of the surface. Five thermocouples, positioned just upstream/downstream of the tube inlet/outlet were used to measure the entering/exiting bulk temperature.

Electric power was supplied to the test section heating wire by one circuit. The source of power for this circuit was an autotransformer, supplied from a standard 220 V, 60 cycle a.c. wall outlet. These autotransformers

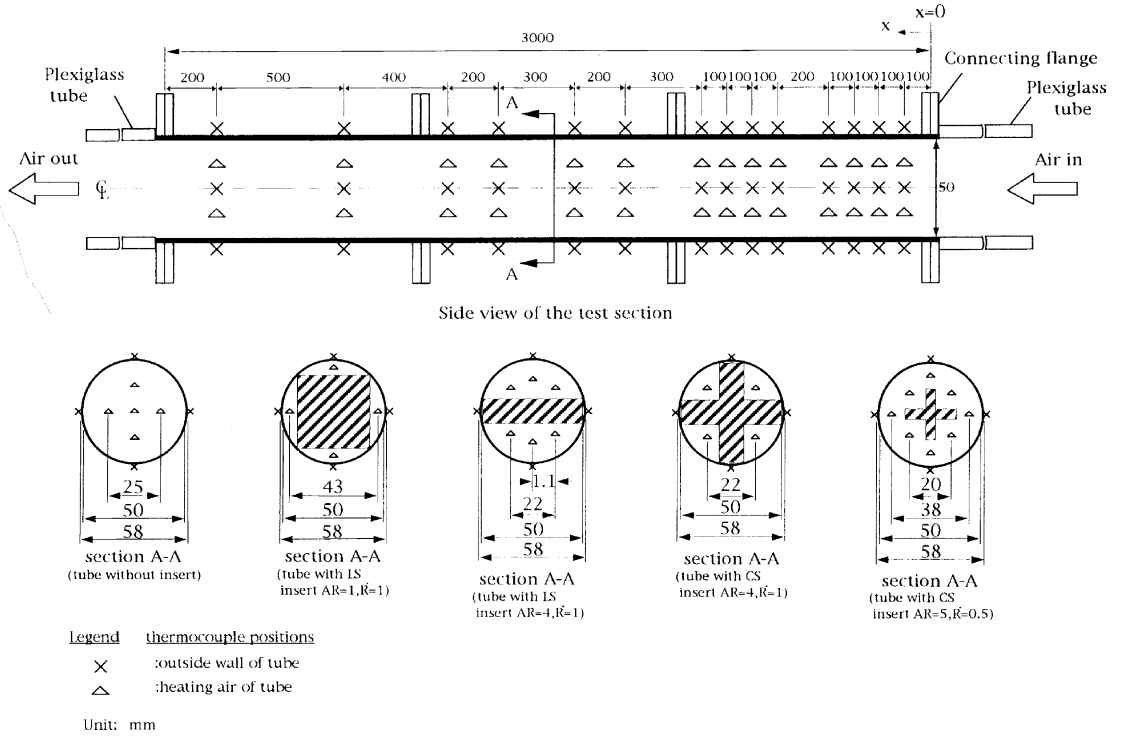

Fig. 3. Thermocouple measuring position for temperature measurements.

were designed for a load voltage output of 0–220 V, with a maximum current of 10 A.

Air flows were measured by an orifice type flowmeter ($\beta = 0.5$) with corrections applied for the temperature range covered during this study. This gives the tube side Reynolds number from 6500 to 19 500. The pressure drop along the test section was measured by means of static manometer. These were connected to pressure taps at each specified downstream distance. The pressure taps were perpendicular to the tube surface. All measurements were made under steady-state conditions. The fluid properties were calculated as the average between the inlet and outlet bulk temperature. Generally, it usually took 30 min to reach steady state at $Re = 6500$.

3. Data reduction

The primary goal of this experiment was the determination of fully developed Nusselt number for air flowing in a horizontal tube with strip type inserts. In addition, buoyancy effect as well as performance evaluation of this type of heat exchanger was also extensively studied. The independent parameters involved in Part II of this paper were the Reynolds number, the Prandtl number and Grashof number. The first parameter was defined and described in Part I of the paper. The Prandtl number of air is about 0.7. The Grashof number for constant heat flux was defined as:

$$Gr^* = \frac{g\beta D^4 q''}{\nu^2 k_f} \tag{1}$$

where q'' is heat flux per unit surface area. The tube side local heat transfer coefficient and Nusselt number due to pure forced convection were calculated as

$$Q_{net} = h_x A_s (T_{wx} - T_{bx})$$

$$Nu_x = \frac{h_x D}{k_f} \tag{2}$$

where k_f is the thermal conductivity of air, A_s is the area of the heated region of the air tubes ($=\pi D_o \ell$), and D_o is the tube outside diameter. The local net heat transfer rate Q_{net} was the electrical power generated from the heater and deducted the heat loss to the outside of the test channel including conduction (about 3% of the input power) and radiation (about 5%) heat losses, and buoyancy effect. T_{wx} was calculated based on the average of several circumferential temperature readings. The local values of the thermophysical properties of air were obtained at the local film temperature (T_f), $T_f = 0.5(T_{wx} + T_{bx})$. The effect of the inserts acting as fins

and modifying the temperature profile of the air in the tube was considered negligible since the plexiglas made insert was chosen.

The determination of fully developed Nusselt number from the experimental data (subtracted the buoyancy effect) begins with the calculation of the overall bulk temperature rise based on energy balance on the flowing air. The energy balance examination was made based on the calculated and measured local air bulk mean temperatures at a particular downstream distance form the inlet and it was found in good agreement within ±5%. The data set consisted of 1750 data points obtained from five different tubes.

4. Experimental uncertainty

An error analysis using the method of Moffat [2] was performed to determine the uncertainty in the experimental data. The single largest contributor to uncertainty in the Reynolds number was the measurement of the volumetric flow rate. The resulting maximum uncertainty in *Re* is 8.2%. The majority of the error in *Nu* can be traced to the uncertainty in the convective heat transfer is due mainly to the simplified analysis for the conduction loss correction. Although the conduction loss through the insert can probably be estimated to within 2–3% accuracy, these losses are so small that it might be negligible. The estimated error in the temperature difference 0.2 °C. The resulting maximum uncertainty in *Nu* is 8%.

5. Results and discussion

Based on hydrodynamic considerations, the flow field is significantly influenced by insert blockage and the secondary flow circulation. The insert increases the wetted perimeter and reduces the flow cross-sectional area.

5.1. Temperature distributions

A representative dimensionless temperature distribution ($Re = 16250$, $Q_{net} = 1370$ W) plot is shown in Fig. 4. In this figure, the ordinate variable is the nondimenionalized temperature difference $((T - T_{bi})/(Q_{net}/\ell k_f))$. The abscissa variable in Fig. 4 is known as the inverse

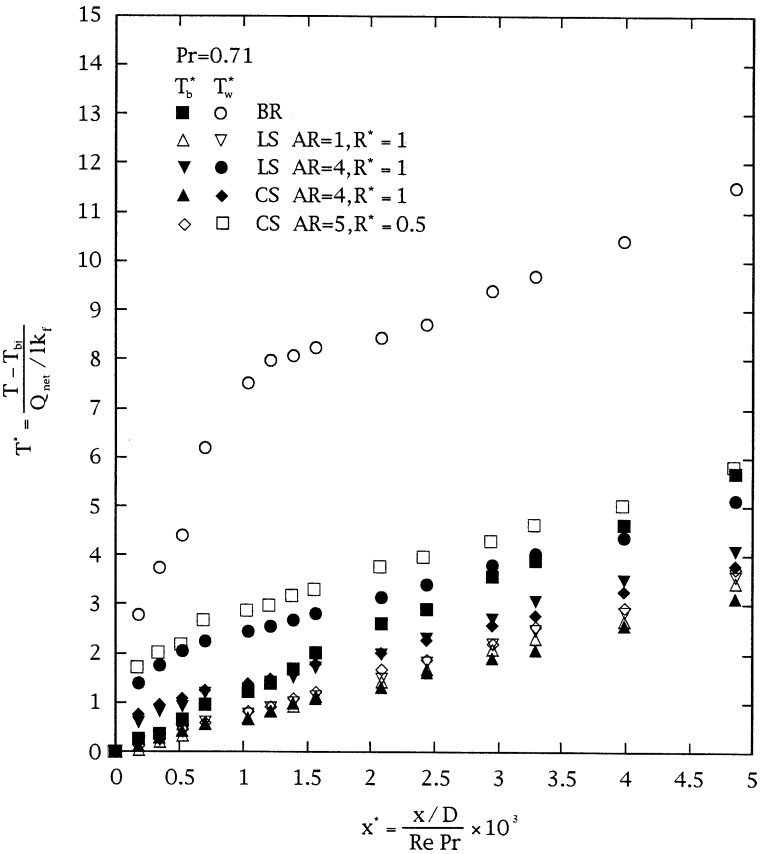

Fig. 4. Local dimensionless wall and bulk temperature distribution at $Q_{net} = 1370$ W, $Re = 16250$.

Graetz number and is a dimensionless representation of the linear axial coordinate.

For the longitudinally constant heat flux boundary condition of the present study, the thermally fully developed region is characterized by wall and bulk mean air temperature that increased linearly as a function of longitudinal downstream position. The most important portion of the wall temperature distribution is the central portion ($x^+ \geqslant 1.5$ for all the cases considered) through which a straight line has been fitted parallel to the line representing the bulk temperature. The vertical distance between this line segment and the bulk temperature line indicates the wall-to-bulk temperature difference used to calculate the fully developed heat transfer coefficient.

From Fig. 4, one can see that the bare tube has the biggest vertical distance, following by LS (AR = 4), CS (AR = 5), CS (AR = 4) and LS (AR = 1). Keeping the other parameters fixed, the smallest vertical distance in Fig. 3 indicates the best heat transfer performance one may obtain. This is partly because LS insert with AR = 1 provides a larger heat transfer area due to the surface of the insert and partly because LS inserts with AR = 1 have a higher convective heat transfer due to a higher average velocity as stated in Part I of this paper. In fact, the ratios of surface area of the tubes with/without inserts are 1.94 for LS (AR = 1), 2.3 for CS (AR = 4), 1.8 for LS (AR = 4), and 1.66 for CS (AR = 5), respectively. For instance, at $Re = 19\,500$, the increase in heat transfer coefficient due to heat transfer area is counterbalanced by the lower heat transport capability due to a lower average velocity for CS insert ($u_0 = 28.6$ m/s for AR = 4) as stated in Part I of this paper compared to the LS inserts ($u_0 = 30.4$ m/s for AR = 1). At this stage, the present enhancement seems strictly due to a combination of the higher heat transfer area, higher heat transport capability (higher average velocity), and a difference in flow patterns when tube was inserted.

The departure of the wall temperature data from straight line behavior at the upstream of the tubes in Fig. 4 was partly due to the absence of front-side heating at this end and partly due to the flow development in the entrance region and small extraneous conduction loss. Nevertheless, the nature of the fully developed heat transfer region can still be observed in the temperature distribution for all the cases under study.

5.2. Law of the wall for thermal boundary layer

Correlation of the law of the wall was based on the temperature distribution measurements in the fully development regions for different values of *Re* as shown in Fig. 5. Assume that, as stated earlier, the Prandtl number (*Pr*) is constant (taken as 0.7) for the present study, it can be correlated in the form of

$$T^+ = 2.19 \ln\left(\frac{y^+}{\eta}\right) + 13.2Pr - 5.66 \tag{3}$$

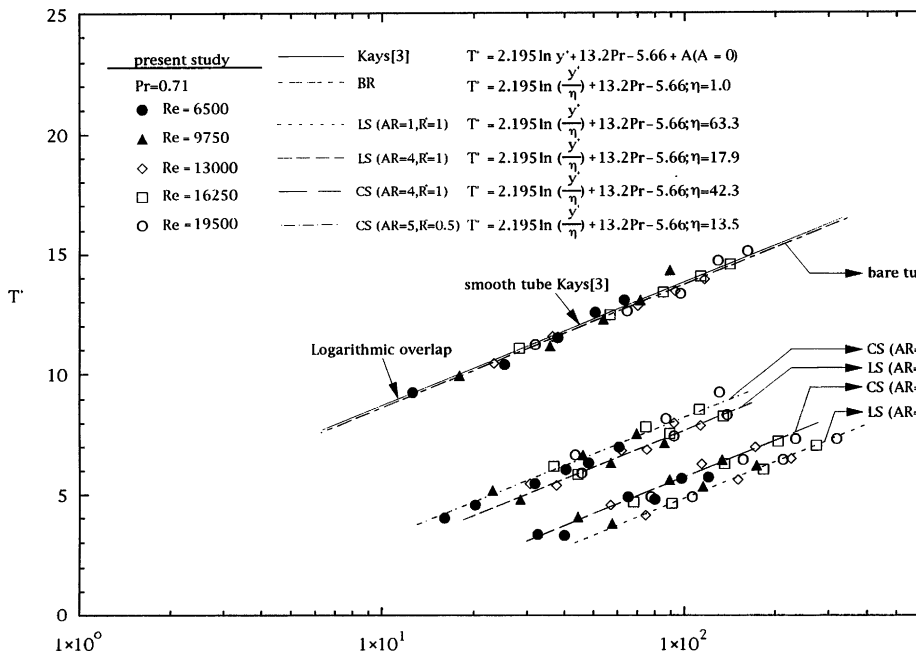

Fig. 5. Law of the wall for temperature distribution in the fully developed region at $Q_{net} = 1370$ W.

when T^+ is nondimensional temperature defined as $(T_w - T)/(q''/\rho C_p u^*)$ and η ($\geqslant 1$), is the insert affected coefficient that determines the shift in the smooth-wall logarithmic temperature profile caused by the present insert and is 1 for a smooth surface.

From Fig. 5 one can see that lines will shift downward from the correlation obtained by Kays and Crawford [3] and the present experiments for bare tube (the deviation $\leqslant 2\%$ for A) with four tubes with inserts. Again, the biggest shift happens for LS (AR = 1, $R^* = 1$) which is consistent with the previous findings in Fig. 4. Naturally, as one would expect, CS (AR = 5, $R^* = 0.5$), LS (AR = 4, $R^* = 1$) and CS (AR = 4, $R^* = 1$) are again located in between. The sequence is a little bit different from the plot of law of the wall for velocity profile in Part I of this paper. This may be caused by temperature effect and consequently, it may be due to buoyancy effect.

5.3. Heat transfer results

5.3.1. Local total Nusselt number ($Nu_{m,x}$) vs. Nu_o and buoyancy effect

Fig. 6 shows the buoyancy effect on the local total (including buoyancy effect) Nusselt number in the entrance as well as fully developed region of a horizontal tube with longitudinal/crossed-strip inserts. It is found that buoyancy effects are practically important at $x/D \leqslant 20$ especially for the bare tube at a higher heat flux level ($Q_{net} = 2055$ W) and $Re = 6500$. In fact, it is found that Gr^*/Re^2 is about 2.24 at this stage. From then on Nu decreases approximately uniformly as it behaves in pure forced convection. Moreover, the buoyancy effects become small when the tube was with insert as well as at high Re and Nu_o was calculated based on Dittus and Boelter formula.

Nevertheless, the buoyancy effect shares its contribution in the heat transfer mechanism and, consequently, this also reflects the importance of buoyancy in developing flow in horizontal tubes especially for tubes without inserts.

Fig. 6(a) shows that the present bare tube heat transfer result is almost the same as Dittus–Boelter's result ($Nu_{m,x}/Nu_o \approx 1$). The deviation may be mainly caused by buoyancy effect especially for $Re = 6500$. The remainder of Fig. 6 does show the enhancement effect of about 2–2.5 times the bare tube for CS and LS inserts.

In the present study different heat flux levels are used to generate different buoyancy effects while keeping the other parameters unchanged.

The measurements were performed at five different Reynolds number for five tubes studied as shown in Fig. 7. In these figures the mean Nusselt number defined as

$$\overline{Nu}_m = \frac{Q}{A}\left[\frac{1}{\ell}\int_o^{\ell}\frac{dx}{T_{wx} - T_{bx}}\right]\left[\frac{D}{k_f}\right] \tag{4}$$

is plotted against the quotient Gr^*/Re^2 at a specific Reynolds number where Q was considered only conduction and radiation heat losses deducted.

From Fig. 7, buoyancy effects are clearly noted at $Re \leqslant 6500$ for bare tube and tube with inserts of CS (AR = 5, $R^* = 0.5$) where there is a positive effect of buoyancy on heat transfer and a big Gr^*/Re^2 ($\cong 1$) for bare tube. Strictly speaking, even at $Re = 19\,500$, Gr^*/Re^2 is for bare tube still higher ($\cong 0.1$–0.3) where mixed convection holds. Since the air is uniformly circumferentially heated in the tube, the fluid near the outer wall is warmer than the bulk fluid in the core. This is because for CS inserts (AR = 5, $R^* = 0.5$), four upward currents flow along half the side walls and have a relative high buoyancy as compared to the rest of tubes with inserts.

5.3.2. Local Nusselt number (Nu_x) vs. Nu_o

Fig. 8 shows the pure forced convection results along the downstream distance for all the tubes under study. The forced convection data were obtained from the following relation [4,5]:

$$Nu_x = (Nu_{m,x}^3 - Nu_{n,x}^3)^{\frac{1}{3}} \tag{5}$$

The natural convection results were secured when short off the power of supply for driven motor. The decrease in Nusselt numbers along downstream direction in the entrance region of the passage shown in Fig. 8 could be considered as the entrance effect, where thermal boundary layer and the turbulence induced by the inserts or the combination of the inserts has not yet been fully developed. The heat transfer enhancement effect was clearly noted for the tubes with inserts. It was found that LS (AR = 1, $R^* = 1$) has the best heat transfer performance. The onset of fully developed value could also be determined from this plot as ranging from $4D$ to $16D$ depending on the tube inside geometry (see Fig. 8 for details). The sequence is similar to that of hydrodynamic entrance length reported in Part I of this paper. Generally, Nu_x/Nu_o keeps above a value of 1.5 for all the tubes with the inserts for the entire length of the tube. Again, the present inserts contribute to continuous interruption (starting right at the inlet of the tube) of the development of boundary layer (LS) as well as to generate the secondary flow (CS) and increased mixing (both types of inserts) resulting in higher heat transfer coefficients as compared to the tubes without inserts.

5.3.3. Developing Nusselt number and Reynolds number dependence

To examine the enhancement provided by the tubes with inserts, comparisons of the present fully developed Nusselt numbers with those for bare tube were also made in Fig. 9. The comparison, shown in Fig. 9 demonstrates the level of heat transfer enhancement

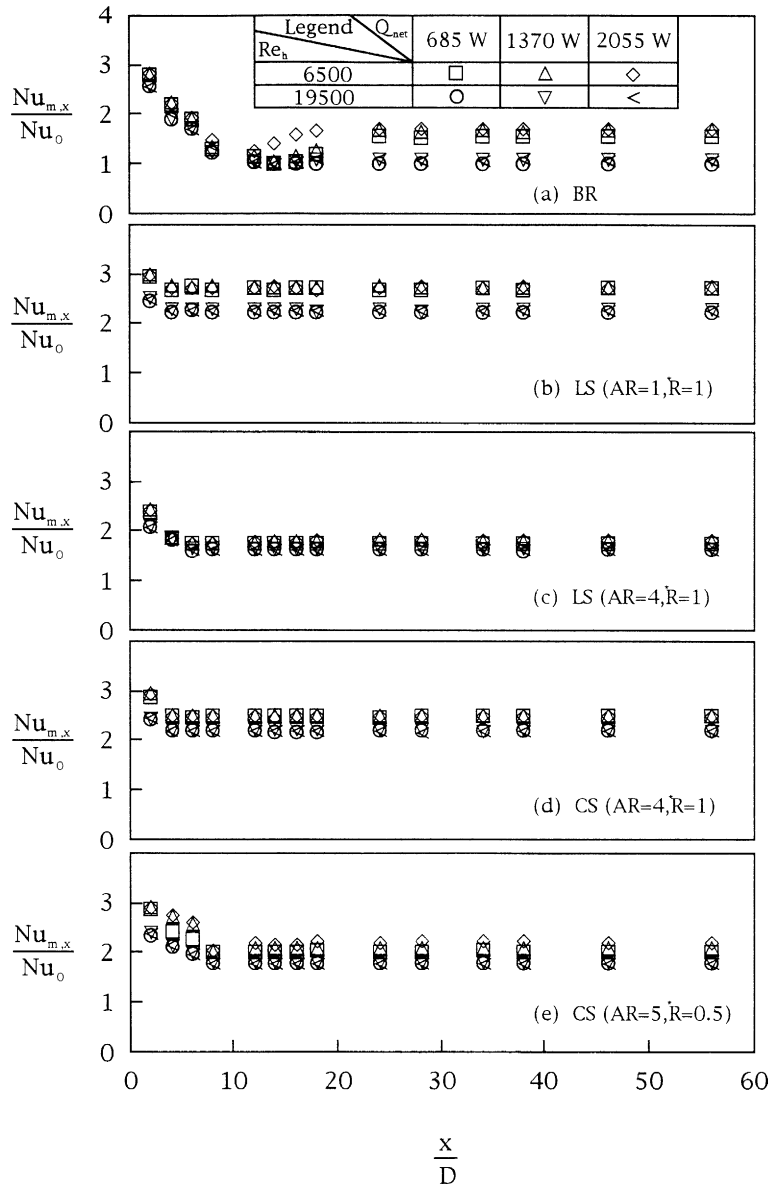

Fig. 6. Nusselt number ratio distribution along downstream direction for different Reynolds numbers and heat input.

associated with the tubes with inserts. This is because the tube with insert provides more heat transport opportunity for a given flow cross-section and a higher local average velocity. The enhancement factor ranges from a minimum of 2.5 at $Re = 19\,500$ to a maximum 3.5 at $Re = 6500$ for LS (AR = 1, $R^* = 1$) which happens to be having the best heat transfer performance. Generally, the enhancement decreases with an increase in Reynolds number for all the tubes with inserts. As stated earlier, fluid flow in tubes with CS inserts provides more heat transport opportunity. However, it is found that the increase in heat transfer coefficient due to heat transfer area is sometimes counterbalanced by the lower local average velocity, compared to CS inserts. Therefore, only AR = 1 with LS insert, could this effect be observed.

Five sets of data were obtained, each set consisting of five data runs at varying Reynolds numbers but at nearly equal Prandtl numbers. A composite power law curve fit was performed to establish a Nusselt–Reynolds relation for each data set. The Nusselt number dependence on Prandtl number was assumed to be the same as for bare tube. A general correlation for $\overline{Nu}$ of Re, D/ℓ, and AR (aspect ratio) was developed for inserted tubes.

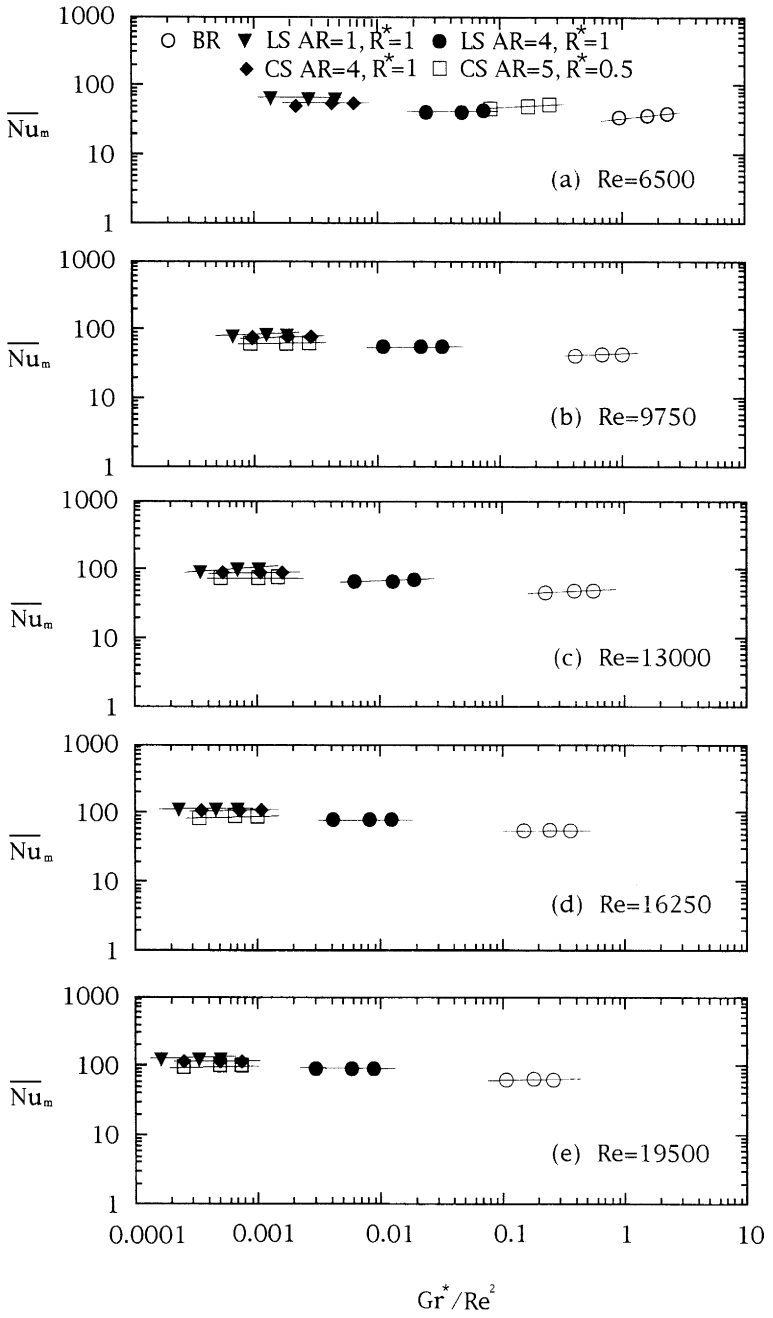

Fig. 7. Buoyancy effect on heat transfer in a horizontal circular tube with different strip inserts.

Fig. 10 presents the present *Nu* correlated with the relevant parameters such as *Re*, D/ℓ, and *Ar*. The influences on *Nu* with *Re*, D/ℓ and *Ar* are quite significant as one noted the magnitude of the power dependence. The increase in *Re* and D/ℓ would result in a *Nu* increase. However, *Nu* decreases as AR increases. An overall Reynolds number dependence of 0.742 was finally determined. The value (=0.742) of the Reynolds number exponent appears low when compared to the 0.8 exponent for a standard turbulent duct flow situation. This finding is expected, however, since the flow in tubes with inserts contains certain zones of recirculation not present in conventional duct flows. In spite of this, the present bare tube result with a Reynolds number

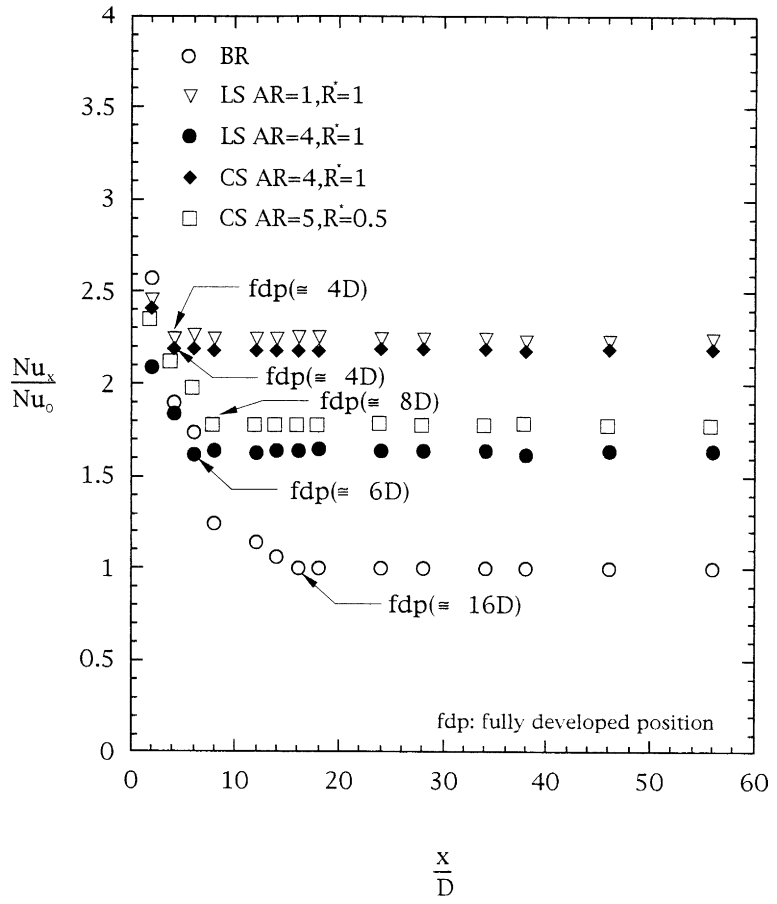

Fig. 8. Local Nusselt number ratio distribution along downstream direction for different strips.

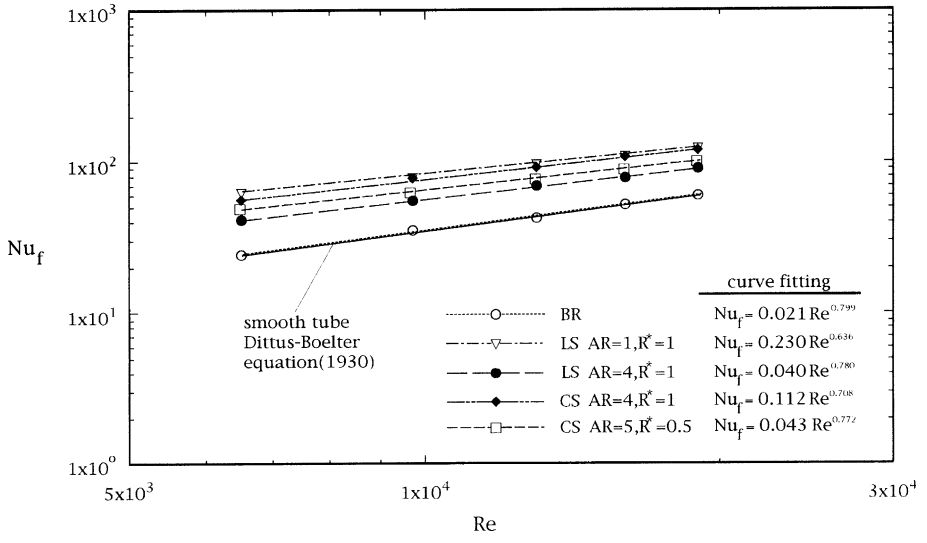

Fig. 9. *Nu* vs. *Re* for different strips.

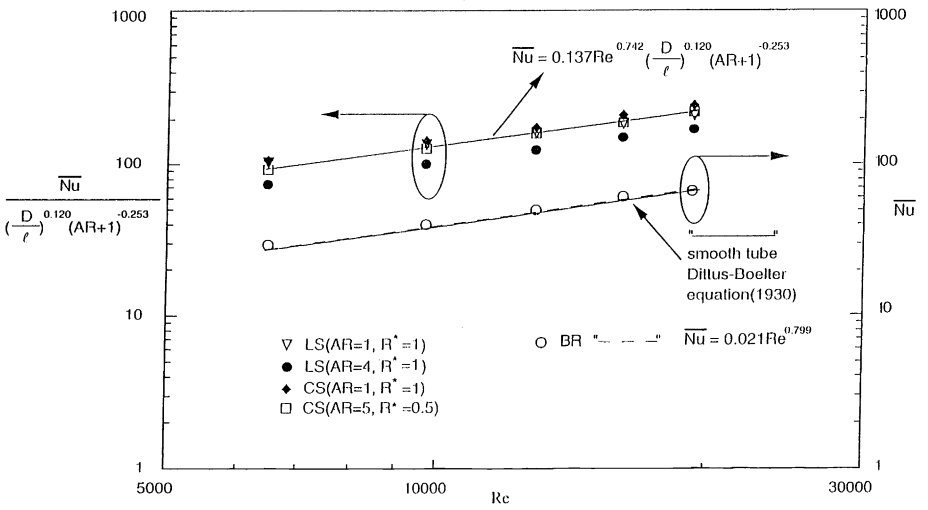

Fig. 10. A correlation of Nusselt number for four different inserted tubes and comparision of Nusselt number correlation for bare tube.

dependence of 0.799 shows an excellent agreement with that of Dittus–Boelter (see Fig. 9 for details). Further examining the effect of D/ℓ, the present insert length has an opposite effect on Nu. The reasons are the same as previously stated for a lower Reynolds number dependency (=0.742). The longer insert results in more zones of recirculation.

5.4. Overall tube performance

Bergles et al. [6] suggested several criteria for the performance evaluation of enhanced tubes. The performance of the insert with the present geometry configurations has been evaluated on the basis of two important criteria, $R1$ (pumping power fixed – increase of heat transfer) and $R2$ (heat duty fixed – reduced pumping power) where $R1 > 1$ and $R2 < 1$ represent enhanced performance. The $R1$ and $R2$ are defined in the following:

$$R1 = \frac{(Nu)_{\text{in}}}{(Nu)_{\text{BR}}} \tag{6}$$

$$R2 = \frac{(fRe^3A)_{\text{in}}}{(fRe^3A)_{\text{BR}}} \tag{7}$$

where the subscripts "in" and "BR" in Eqs. (6) and (7) stand for insert and bare tube, respectively. The detailed evaluating procedure can be referred to Hsieh and Kuo [7]. Fig. 11 shows the variation of the performance ratios of $R1$ and $R2$, respectively, with equivalent bare tube Reynolds number Re. The relationship between f and Re can be obtained from Part I of this paper. Amongst of tubes, LS (AR = 1, $R^* = 1$) shows an improvement of 340% in heat transfer coefficient at lower values of Re ($\leqslant 9750$), compared to 280% only at higher Re values ($\geqslant 16\,250$), while CS (AR = 5, $R^* = 0.5$) gives the least improvement of 50–60% over the entire range of Re. Moreover, for all the tubes with inserts studied, performance ratio of $R1$ was generally found to decrease with an increase in Re. This trend was also observed by Uttarwar and Rao [8]. Also shown in Fig. 11 is the performance ratio of $R2$. The results indicate that a reduction as high as 60–90% can be obtained in heat transfer area using LS (AR = 1, $R^* = 1$) and CS (AR = 4, $R^* = 1$), while the reduction is only about 30% for CS (AR = 5, $R^* = 0.5$). In general, $R2$ increases as Re increases in the present study. Additionally, it is interesting that the performance between LS (AR = 1) and CS (AR = 4) are so close to each other but so much higher than LS (AR = 4) and CS (AR = 5).

Based on $R1$ and $R2$, it is suggested that tubes with LS perform better than the tubes with CS especially at lower Re values.

6. Conclusion

Experimental measurements for a developing turbulent convection in an axially/circumferentially uniformly heated horizontal tube with different longitudinal inserts for a Pr of 0.7 was conducted. The investigation of the effects of various parameters, such as Reynolds number (Re), Grashof number (Gr), aspect ratio (AR) and radius ratio (R^*) of the insert on heat transfer and thermally entrance length in the developing and fully developed

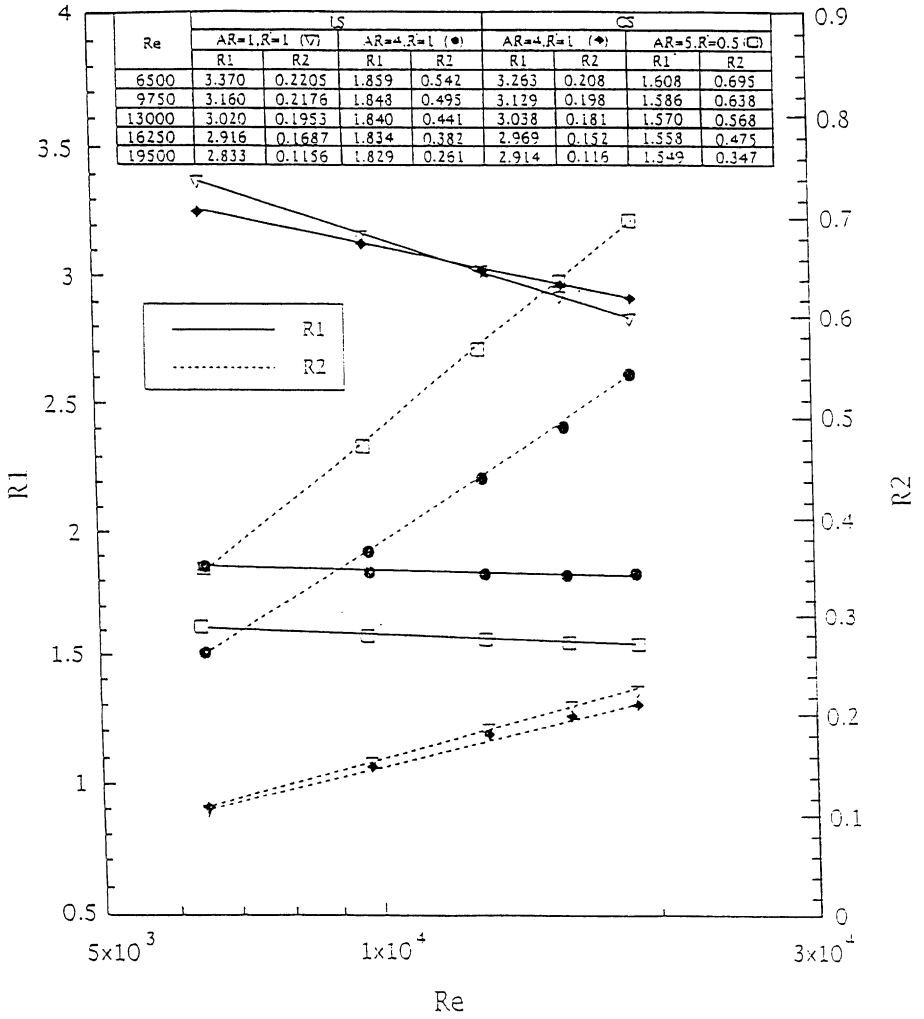

Fig. 11. Thermal performance of four different tube with inserts compared with bare tube based on criterion 1 and criterion 2.

regions were extensively studied. Most salient features were drawn in the following:

1. The thermally entrance length and buoyancy effects becomes smaller for tubes with inserts.
2. Law of the wall for temperature profile was first made for this type of enhancement device for $6500 \leqslant Re \leqslant 19\,500$.
3. The heat transfer enhancement of the tubes with inserts is about four to two times that of bare tubes for $Re = 6500$ to 19 500.
4. Overall performance was evaluated based on $R1$ (constant pumping power) and $R2$ (constant heat duty). Both show that the tubes with inserts are beneficial as far as economics is concerned. As a result, an optimum operating condition could be thus obtained.

References

[1] S.-S. Hsieh, F.Y. Wu, H.H. Tsai, Turbulent heat transfer and flow characteristics in a horizontal circular tube with strip-type inserts. Part I. Fluid mechanics, Int. J. Heat Mass Transfer, PII: S0017-9310(02)00353-8.

[2] R.J. Moffat, Describing the uncertainties in experimental results, Exp. Thermal Fluid Sci. 1 (1988) 3–17.

[3] W.M. Kays, M.E. Crawford, Convective Heat and Mass Transfer, second ed., McGraw-Hill, New York, 1980 (Chapter 13).

[4] S.-S. Hsieh, M.-Y. Wen, Developing three-dimensional laminar mixed convection in a circular tube inserted with longitudinal strips, Int. J. Mass Transfer 39 (2) (1996) 299–310.

[5] F.M. White, Heat and Mass Transfer, Addison Wesley, New York, 1988, p. 415.

[6] B.E. Bergles, A.R. Blumenhrontz, J. Taborek, Performance evaluation criterion for enhanced heat transfer surfaces, Proc. Int. Heat Mass Transfer Conf. 2 (1974) 239–243.
[7] S.-S. Hsieh, M.-T. Kuo, An experimental investigation of the augmentation of tube-side heat transfer in a crossflow heat exchanger by means of strip-type inserts, ASME J. Heat Transfer 116 (2) (1994) 383–390.
[8] S.B. Uttarwar, R.M. Rao, Augmentation of laminar flow heat transfer in tubes by means of wire coil inserts, ASME J. Heat Transfer 107 (1985) 930–935.